RESEARCH ARTICLE
SOLID EARTH: GEODYNAMICS

Earth and Planetary Physics
9: 1011–1021, 2025
doi: 10.26464/epp2025077

Central American slab tearing controlled by lateral pressure force due to former Farallon subduction

Jian Wang[1,2], LiJun Liu[1*], YanChong Li[3], ZeBin Cao[1], and Hao Dong[1]

[1]State Key Laboratory of Lithospheric Evolution, Institute of Geology and Geophysics, Chinese Academy of Sciences, Beijing 100029, China;

[2]College of Earth and Planetary Sciences, University of Chinese Academy of Sciences, Beijing 100049, China;

[3]Department of Earth Science and Environmental Change, University of Illinois at Urbana-Champaign, Urbana, Illinois 61801, USA

Key Points:

- Seismic observations reveal a complex structure of the subducting Cocos slab.
- We used four-dimensional data assimilation models to reproduce the complex configuration of the Cocos slab.
- The lateral pressure gradient induced by the ancient Farallon Slab helped cause repeated tearing and subduction of the Cocos slab.

Citation: Wang, J., Liu, L. J., Li, Y. C., Cao, Z. B., and Dong, H. (2025). Central American slab tearing controlled by lateral pressure force due to former Farallon subduction. *Earth Planet. Phys.*, *9*(5), 1011–1021. http://doi.org/10.26464/epp2025077

Abstract: Subduction zones are major convergent boundaries, where the downgoing oceanic plates usually form continuous tabular slabs extending deep into the Earth's interior. However, many subducting slabs especially those with young ages, exhibit complex geometry, with varying degrees of influence on the overlying continent and surface environment. To better understand the mechanism of such slab deformation, we apply four-dimensional finite element geodynamic models with data assimilation to investigate the evolution of the Cocos subduction in Central America, where a double-slab configuration with complex tearing has recently been observed. We reproduce the subduction history of the Cocos slab since the Eocene. During this period, multiple episodes of tearing occurred within the Cocos slab, starting at 25 Ma. We find that the ancient Farallon slab, subducted during the Mesozoic, enhances the lateral pressure gradient across the slab hinge, promoting eastward mantle flow and tearing of the Cocos slab. The repeated tearing and subduction of the young Cocos plate have shaped the complex slab configuration in the region.

Keywords: subduction; slab tearing; Cocos slab; lateral pressure gradient; mantle wind

1. Introduction

The theory of plate tectonics posits that the oceanic lithosphere is rigid and may maintain its high mechanical strength even during subduction, thus forming a simple slab morphology for an extended period after subducting into the mantle at convergent margins. This understanding aligns with numerous fundamental observations in subduction zones, such as linear island arcs and smooth Benioff zone geometry (Stolper and Newman, 1994; Hyndman et al., 1997). However, with the continuous advancement of seismic imaging techniques, slab tearing has increasingly been observed beneath various subduction zones. Examples include the African slab beneath the Aegean Sea (Jolivet et al., 2015), the western Pacific slab beneath the Mariana Trench (Miller et al., 2006; Obayashi et al., 2009), the Farallon slab beneath western North America (Schmandt and Humphreys, 2010), and the Cocos slab beneath Central America (Rogers et al., 2002). Additionally, integrated studies combining geological records, geophysical data, and geodynamic simulations have revealed similar slab tearing events in the past, such as those in southwestern Gondwana during the Mesozoic (Gianni et al., 2019) and in North America (Liu LJ and Stegman, 2011) and South America (Hu JS et al., 2017) during the Cenozoic.

There remains considerable debate regarding the mechanisms of slab tearing. Previously proposed models have included mantle flow and plate rotation (Jolivet et al., 2015; Gianni et al., 2019), direct interaction with nearby slabs or with the ambient mantle (Miller et al., 2006; Obayashi et al., 2009), erosion and destruction of subducting slabs by mantle plumes (Obrebski et al., 2010; Zhou Q et al., 2018b), and reactivation of preexisting weak zones within the downgoing slab (Hawley and Allen, 2019). However, because these models are mostly qualitative, their applicability to slab tearing observed in different regions remains uncertain. Given the widespread occurrence of slab tearing, further exploration of its mechanisms could enhance our understanding of complex slab morphology, providing deeper insight into how subduction processes affect the overriding plates and the surface environment.

In this study, we investigate the dynamic mechanisms of slab tearing by constructing quantitative dynamic models to simulate the evolution of subducting slabs. Our research focuses on Central

First author: J. Wang, wangjian37@mail.iggcas.ac.cn
Correspondence to: L. J. Liu, ljliu@mail.iggcas.ac.cn
Received 01 MAR 2024; Accepted 07 MAY 2025.
First Published online 07 JUL 2025.
©2025 by Earth and Planetary Physics.

America, where the region has primarily been influenced by the subduction of the young Cocos slab since the early Cenozoic (Müller et al., 2019). The relatively simple subduction history and the young subducting plate in this region are conducive to the formation of slab tearing (Liu LJ and Stegman, 2011) and facilitate a systematic analysis of the associated dynamic processes.

2. Tectonic Setting and Mantle Structure of Central America

The Cocos Plate is situated to the west of Central America, bordered by the East Pacific Rise to the west and the Nazca Plate to the south. The Cocos Plate was formed by the spreading of the Pacific–Cocos Ridge and the Cocos–Nazca Ridge. Along with the Nazca Plate, the Cocos Plate is a remnant of the ancient Farallon Plate, which fragmented approximately 23 million years ago (Xue T et al., 2023). It exhibits a triangular morphology, subducting northeastward beneath the American Plate and the Caribbean Plate. Seafloor magnetic anomaly data reveal that the subduction rate of the Cocos Plate since the Neogene has shown an increasing trend from north to south along the Middle America Trench (Rogers et al., 2002).

Cocos subduction is accompanied by frequent seismic activity near the trench and substantial topographic uplift within the overriding Central American and Caribbean Plates (Figure 1a). Rogers et al. (2002) first identified a slab gap along the Middle America Trench through P-wave imaging. Liu M and Gao HY (2023) utilized full-waveform ambient noise tomography to show that the reduction in seismic velocity during the transition from steep to flat subduction likely represents slab tearing. Another recent imaging study revealed that the Cocos slab has a more complex structure, with two separate branches of fast anomalies beneath the region (Zhu HJ et al., 2020; Figures 1b and 1c). This configuration is consistent with a previous receiver-function study that proposed a double-subduction model with opposite polarities, where the Cocos slab truncated another west-dipping slab to the east (Kim et al., 2011). Therefore, the nature and formation of the Central American slab structure remains elusive.

However, seismic imaging results do not directly reveal the evolutionary history of slab tears. Xue T et al. (2023) simulated the subduction of the Cocos slab beneath Central America by using shear-wave splitting and dynamic modeling, which suggested that slab tearing began approximately 10 million years ago. They argued that the relatively young Cocos slab, with its high temperature and low mechanical strength, cannot withstand the pressure gradient across the slab, leading the slab to tear. However, this study did not explain the source of the pressure gradient or how its variation affects the process of slab tearing, leaving the ultimate mechanism open for further investigation.

Although slab tearing has been observed and studied in various subduction regions, the tearing of the Cocos slab beneath Central America, despite being repeatedly detected by seismic imaging, has received limited attention in dynamic modeling. Moreover, the fundamental mechanisms underlying slab tearing remain poorly understood.

3. Method

To reconstruct the evolutionary mantle process of the Central

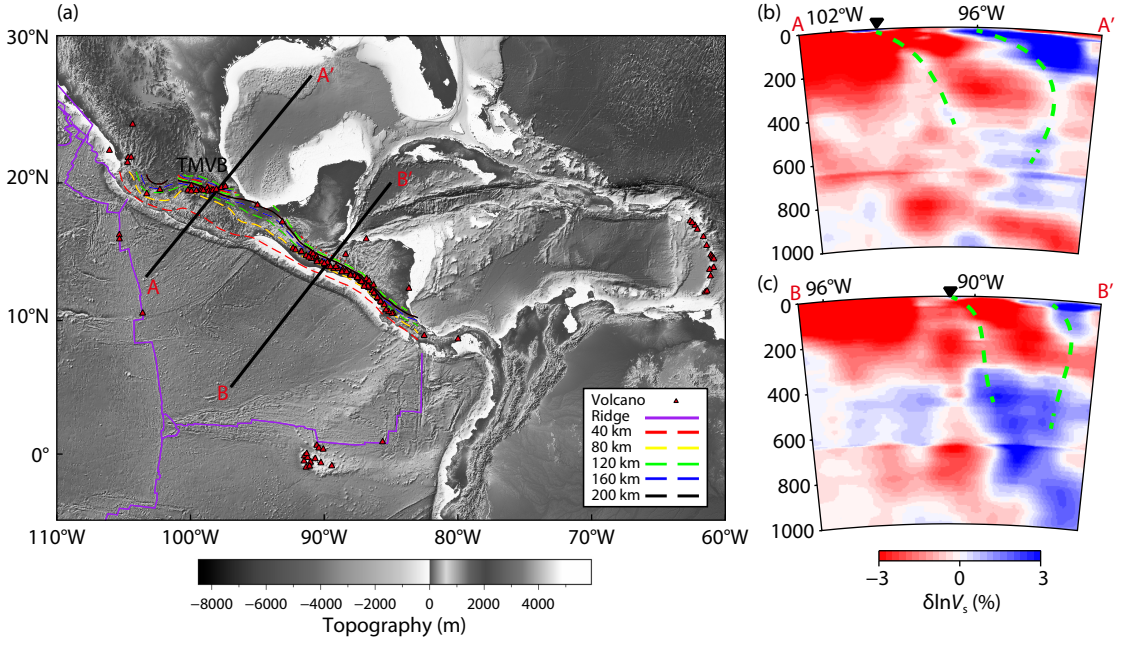

Figure 1. Tectonic and seismological background of Central America. (a) Grayscale topographic map of Central America, where the red triangles represent active volcanoes and the solid purple line indicates the mid-ocean ridge. Volcano locations are sourced from Rogers et al. (2002), and the ridge location is from Müller et al. (2019). The dashed colored lines denote subducting slabs at varying depths, with slab depth data sourced from Hayes et al. (2018). Profiles A–A′ and B–B′ in panel (a) correspond to panels (b) and (c), respectively. (b) Seismic tomography profile along A–A′. (c) Seismic tomography profile along B–B′. The imaging data for (b) and (c) are from Zhu HJ et al. (2020). The dashed green lines in (b) and (c) show the highly distorted or torn upper-mantle slabs.

American region since the Eocene, this study follows the approach of modeling South American subduction in Hu JS et al. (2017) and utilizes the three-dimensional (3D) finite element code CitcomS (Zhong SJ et al., 2000; Tan E et al., 2006) to establish a subduction model of Central America.

3.1 Governing Equations

CitcomS is a finite element program for solving thermal convection problems in spherical shells relevant to mantle dynamics. Its fundamental principle involves treating the mantle as a purely viscous, incompressible spherical shell and solving the governing equations of thermal convection (i.e., the conservation of mass, momentum, and energy):

$$\nabla \cdot \boldsymbol{u} = 0, \tag{1}$$

$$-\nabla P + \nabla \cdot \left[\eta\left(\nabla \boldsymbol{u} + \nabla^{\mathrm{T}}\boldsymbol{u}\right)\right] + \left(\rho_m \alpha \Delta T + \Delta\rho_c\right)\boldsymbol{g} = 0, \tag{2}$$

$$\frac{\partial T}{\partial t} + \boldsymbol{u} \cdot \nabla T = \kappa \nabla^2 T, \tag{3}$$

$$\frac{\partial C}{\partial t} + \boldsymbol{u} \cdot \nabla C = 0. \tag{4}$$

In the equations above, $\boldsymbol{u}$ represents velocity, P stands for dynamic pressure, η is dynamic viscosity, ρ_m refers to ambient mantle density, α is the thermal expansion coefficient, $\Delta\rho_c$ represents a compositional density anomaly, $\boldsymbol{g}$ is gravitational acceleration, ΔT represents a temperature anomaly, κ denotes thermal diffusivity and C represnts the composition.

In our model, both compositional and thermal buoyancy are considered to accurately replicate the realistic evolution process of our study region. Additionally, CitcomS utilizes a Lagrangian particle ratio method to describe the advection of chemical particles (Tackley and King, 2003).

3.2 Model Setting

The study area of the model spans a latitudinal range of 40°N to 20°S and a longitudinal range of 40°W to 120°W, encompassing the entire mantle down to the core–mantle boundary. In this study, the research region is discretized into a grid of 512 × 512 × 112 (latitude × longitude × depth). Subduction starts from the Eocene (approximately 45 million years ago) and lasts until the present day. To enhance the resolution of the study area and accurately capture the characteristics of the subducting Cocos slab, the grid is refined in the central part of the model (centered at 80°W and 10°N) and in the shallow region (with the densest elements at the surface, gradually coarsening with depth). The size of the finest grid cells in the model is approximately 12 × 17 × 7 km (latitude × longitude × depth). The key parameters are given in Table 1.

In this study, the top surface of the model adopts the evolving plate motions from Müller et al. (2019) as the velocity boundary condition, whereas all other boundaries are set as free-slip boundaries. Additionally, this study assimilates time-evolving plate boundaries into our model to track the location of the subduction zone. All time-dependent information, such as plate motion and plate boundary coordinates, is spatially and temporally interpolated using the open-source paleogeographic software GPlates (www.gplates.org). This study utilizes seafloor ages from the same plate reconstruction to define and update the thermal profile of the oceanic lithosphere, assuming an error function based on the half-space cooling model. A surface thermal boundary condition of 0 °C is prescribed. By constraining the model with plate reconstruction velocities and seafloor ages at each time step, we ensure that the plate motion history is consistent with observations, thereby reasonably reproducing the evolutionary process of the Central American region since the Eocene.

Table 1. Model parameter setting.

Parameter	Value
Mantle temperature	1400 °C
Mantle density	3340 kg/m^3
Reference viscosity	10^{21} Pa s
Maximum viscosity cutoff	10^{23} Pa s
Minimum viscosity cutoff	10^{19} Pa s
Clapeyron slope at 410 km	4.0 MPa/K
Clapeyron slope at 660 km	−2.0 MPa/K

In this study, we test the dynamic effect of far-field mantle buoyancy structures, such as the former Farallon slab subducted during the Mesozoic, to quantify the forces and mechanisms involved in the evolution of Central American subduction. In particular, by comparing the model results with versus without the former Farallon slab, we analyze the influence of this important far-field factor on the pressure field and mantle flow during the tearing process of the Cocos slab. In our model, the Farallon slab is represented as a low-temperature anomaly in a specific region of the mantle at the initial time. This region is initially defined as a thick slab pile extending from 200 to 800 km in depth, mimicking the plausible configuration of this feature around 40 Ma (Liu LJ et al., 2008; Liu LJ and Stegman, 2011; Zhu HJ et al., 2020), with its temperature set to 1100 °C (compared with the background mantle temperature of 1400 °C). Subsequently, this low-temperature anomaly is allowed to evolve freely over time, which regulates the pressure and flow of the rest of the model domain.

It should be noted that the volume of the Farallon slab is estimated from seismic tomography (e.g., Grand et al., 1997), whereby its location and orientation during the initial time are based on a previous inverse model (Liu LJ et al., 2008) where the present-day Farallon slab was pulled back to the surface (Figure 1). We find that the mere presence of the ancient Farallon slab is key for the dynamics of the Cocos subduction. Relatively speaking, the exact volume or shape (within tomographic uncertainties) of this slab has a lesser effect on the dynamics of the Cocos subduction.

3.3 Rheology

In this study, we adopt a temperature- and composition-dependent viscosity structure. The background viscosity structure is divided into four layers: lithosphere (10^{20} Pa s), asthenosphere (10^{20} Pa s), mantle transition zone (10^{20} Pa s), and lower mantle (1.5×10^{22} Pa s). The rheological parameters used in our data assimilation model are based on numerous previous studies (e.g., Liu LJ and Stegman, 2011, 2012; Hu JS et al., 2016, 2018; Zhou Q et

al., 2018a, b; Peng DD and Liu LJ, 2022) in which various parameters were tested to properly reproduce realistic subduction behaviors and to meet observational constraints. In subsequent simulation, the viscosity of the grid cells is updated through multiple iterations.

The temperature-dependent viscosity is calculated using the following formula:

$$\mathrm{visc} = \mathrm{visc0} \times \exp\left(\frac{\mathrm{visc}E}{T^* + \mathrm{visc}T} - \frac{\mathrm{visc}E}{1 + \mathrm{visc}T}\right), \tag{5}$$

where $T^* = \min(\max(T, 0), 1)$ and T is the nondimensionalized temperature. In our model, the nondimensionalized mantle potential temperature is set to 0.7. In addition, visc0 is the reference viscosity, and $\mathrm{visc}E$ and $\mathrm{visc}T$ are defined by the following equations:

$$\mathrm{visc}E = \frac{E_a}{R\Delta T}, \tag{6}$$

$$\mathrm{visc}Z = \frac{\rho g V_a}{R\Delta T}, \tag{7}$$

$$\mathrm{visc}T = T_0. \tag{8}$$

In the equations above, E_a and V_a represent the activation energy and activation volume, respectively, R is the ideal gas constant, ρ is density, $\boldsymbol{g}$ is gravitational acceleration, ΔT is the temperature drop from the core–mantle boundary to the surface, and T_0 is the temperature at the surface.

For the composition-dependent viscosity calculation, we place particles in each grid cell (in this study, each grid cell contains 35 particles). These particles carry information about the different compositional components defined in the model (Table 2) and move between grid cells as the simulation evolves (Hu JS et al., 2018; Peng DD et al., 2021b). When calculating viscosity, the compositional information carried by the particles in each grid cell is first averaged geometrically based on the proportion of particles. This average is then used to compute the corresponding viscosity coefficient that reflects the composition of the grid cell. The final viscosity of the model is obtained by multiplying the temperature-dependent viscosity by the composition-dependent viscosity coefficient.

4. Results

In this study, we primarily test two models. The first model does not consider the ancient Farallon slab and is referred to as Model 1 in the subsequent text. The second model incorporates the Farallon slab and is referred to as Model 2. Please note that each of these two models requires fine-tuning of model parameters to obtain natural-looking slabs that best match the seismic image. Overall, the models with and without the ancient Farallon slab exhibit significant differences in both the direction and magnitude of mantle flow, particularly in the lower mantle beneath the Cocos slab.

4.1 Results of Model 1

Figure 3 shows temporal snapshots of Model 1 (without the Farallon slab). In this model, the geometry (contours in Figure 3) of the subducting slab is defined as being 200 °C below the background mantle temperature. The isotherms with different colors in Figure 3 represent the Cocos slab at depths from 40 to 200 km. Prior to 30 Ma, the Farallon Plate had not yet fragmented into the Cocos and Nazca Plates. During this period, the subduction zone on the western side of Central America was largely continuous, with no significant distortion or tearing observed (Figures 3a–3c). Beginning from 30 Ma, a slab window began to form in the region where the Cocos Ridge intersects the American continent (present-day Panama) in southern Central America (Johnston and Thorkelson, 1997). By 20 Ma, a slab gap appeared within the northern part of the newly formed Cocos slab, whereas the mid-ocean ridge kept growing next to the slab window in the south. Subsequently, the ridge continued to subduct at this location, and the slab window progressively expanded until the present day (Johnston and Thorkelson, 1997). From 20 Ma onward, the gap in the northern section gradually widened to eventually become a slab window.

Within the central portion of the subduction zone, the slab underwent notable deformation beginning as early as 30 Ma, with multiple phases of strong distortion at various depths. Around 5 Ma, multiple small slab tears developed west of present-day Nicaragua and Honduras near the center of the subduction zone (Figure 3h), where these tears persisted until the present day. We suggest, based on the seismic imaging results (Rogers et al., 2002; Zhu HJ et al., 2020), that the present gaps observed in Central America may correspond to the tearing of the Cocos slab over the past 30 million years (Rogers et al., 2002; Liu M and Gao HY, 2023).

4.2 Results of Model 2

Figure 4 presents the simulation results with the inclusion of the Mesozoic Farallon slab. Compared to Model 1, slab evolution at the northern and southern ends of the subduction zone remains similar, although the continuity of the subduction zone in the

Table 2. The composition components in our model.

Number	Component	Number	Component
0	Ambient mantle	7	Arc-like material
1	Weak oceanic crust	8	Buoyant ocean layer
2	Upper continental crust	9	Ocean eclogite
3	Lower continental crust	10	Ocean plateau
4	Upper continental lithosphere	11	Continental eclogite
5	Mid-continental lithosphere	12	Core–mantle boundary material
6	Lower continental lithosphere		

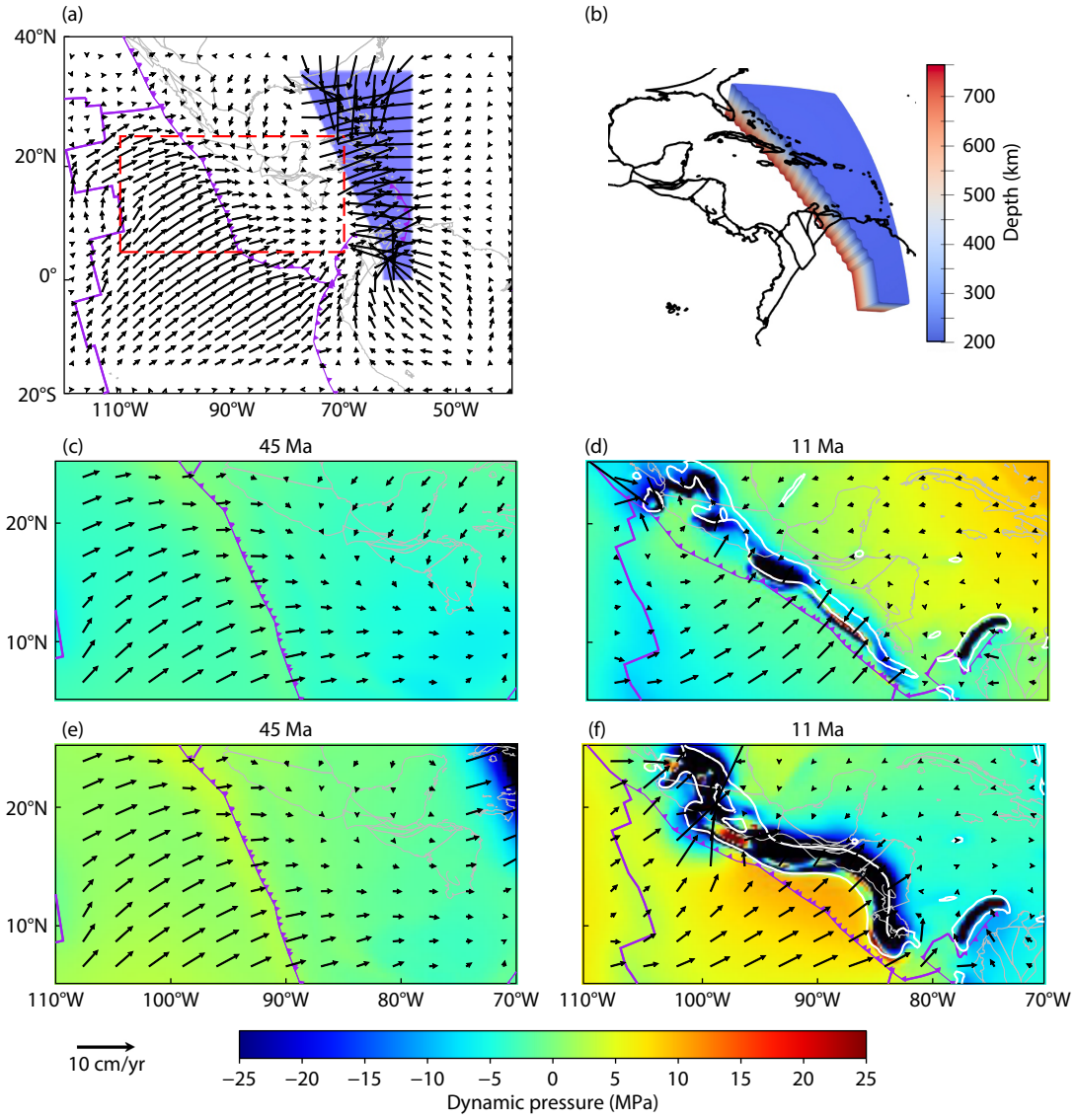

Figure 2. Initial conditions and comparison of the two models for the Central American model. (a) The model region of this study, where the blue polygon represents the horizontal cross-section of the ancient Farallon slab added. Except for the low-temperature region representing the Farallon slab in the initial conditions, all other parameters are consistent between the two models. The dashed red box indicates the region shown in (c) to (f); the solid purple line represents the plate boundary (data from Müller et al., 2019) reconstruction, and the background shows the flow field at a depth of 200 km at the initial time. Panels (c) and (d) show model results excluding the former Farallon slab, whereas panels (e) and (f) present results incorporating the former Farallon slab. (b) The 3D morphology of the ancient Farallon slab in our model. (c) Initial pressure and flow field at a depth of 200 km for the model without the Farallon slab, with panels (d) to (f) using data from the same depth. (d)Pressure and flow field at 11 Ma for the model without the Farallon slab, where the solid white line represents the slab boundary at 200 km depth. (e) Initial pressure and flow field for the model with the Farallon slab. (f) Pressure and flow field at 11 Ma for the model with the Farallon slab. The solid white line marks the 1300 °C isotherm (100 °C below the ambient mantle temperature), representing the thermal boundary of the slab at a depth of 200 km.

northern part of Central America begins to change around 30 Ma (Figures 3c and 4c), forming a slightly larger slab window at the present day than that observed in Figure 3. Slab behaviors within the central portion of the subduction zone show more differences from those in Model 1. For example, the slab dip is notably shallower, as shown by the consistently more landward location of slabs at all depths. Beginning at 30 Ma, a prominent central shallow to flat slab appeared. From 5 Ma, the trenchward part of the flat slab starts to tear, forming a new slab that sinks more steeply into the mantle west of present-day Honduras and Nicaragua, accompanied by a major slab gap between the two slab segments (Figure 4h).

Relative to the multiple small slab tears in Model 1 along the central subduction zone, Model 2 has a single large central slab tear. In addition, Model 2 reproduces a double-slab scenario along trench-normal sections in both the northern and central portions (Figures 4 and 5), whereas Model 1 has this configuration only near the northern edge (Figures 3 and 5). Clearly, Model 2 matches the seismic observations better than Model 1 (Figures 1b

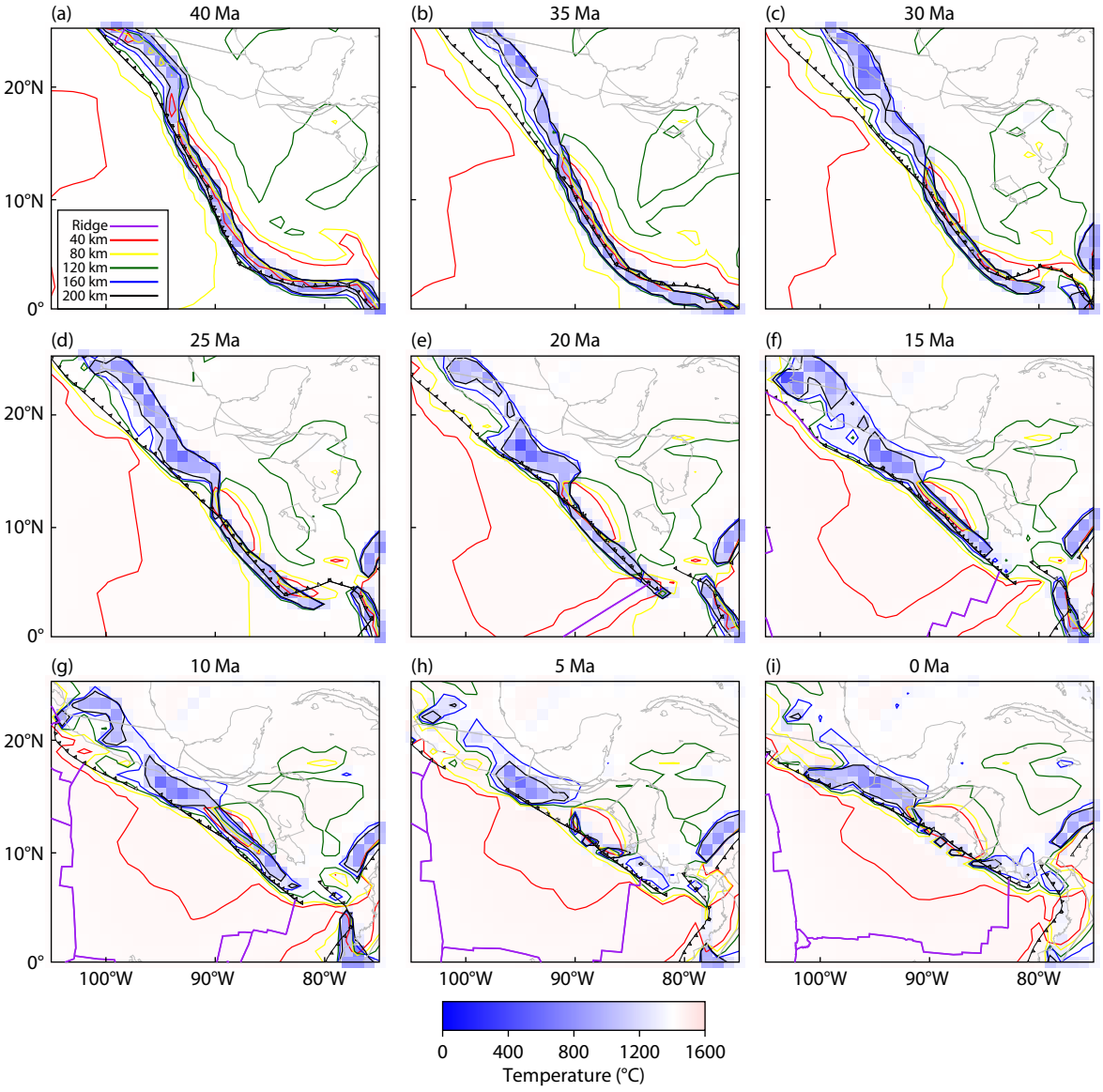

Figure 3. Evolution process of Model 1 (without the Farallon slab). The solid purple lines represent mid-ocean ridges at different times, whereas the solid lines of other colors represent the 1200 °C isotherms (outlining the geometry of the subducting slab) at various depths. The background shows the temperature field at 200 km depth. The mid-ocean ridge and coastline data are sourced from Müller et al. (2019).

and 1c). By combining the seismic observation and model results, we conclude that the inclusion of the ancient Farallon slab strongly alters the subduction process and the final model outcome. Furthermore, the Model 2 results provide a new explanation for the apparently complex slab structure below Central America, without the need to invoke double subduction in the region.

5. Discussion and Conclusions

By comparing the two models above, we identified the important role of the ancient Farallon slab in the evolution of Central American subduction. Physically, the sinking of the Farallon slab east of the Central American trench greatly reduces the dynamic pressure above the Farallon slab, consequently elevating the pressure on the other side of the Central American trench because of the conservation of mass and momentum (Figure 2d vs. 2e). The resulting lateral pressure gradient across the trench pushes the Cocos slab landward and repeatedly tears the slab hinge.

Consequently, our modeled slab behavior and structures differ notably from traditional subduction models. The present-day slab structure looks so complex because of the transient nature of the slab tear. For example, a slab gap such as that near the northern slab edge may be rapidly subducted before another tear forms. The slab geometry along cross-sections A–A′ and B–B′ seems to suggest multiple subduction events of the Cocos slab (Figures 6b–6e) owing to the presence of multiple slab hinges at asthenospheric depths and the apparent separation of slab segments and their imbricated orientation further down. Our models suggest that this unique slab configuration corresponds to slab flattening at shallow depths and repeated opening and subduction of slab tears over time, forming slab doublets across the upper mantle (like a fold but with a structural discontinuity between different

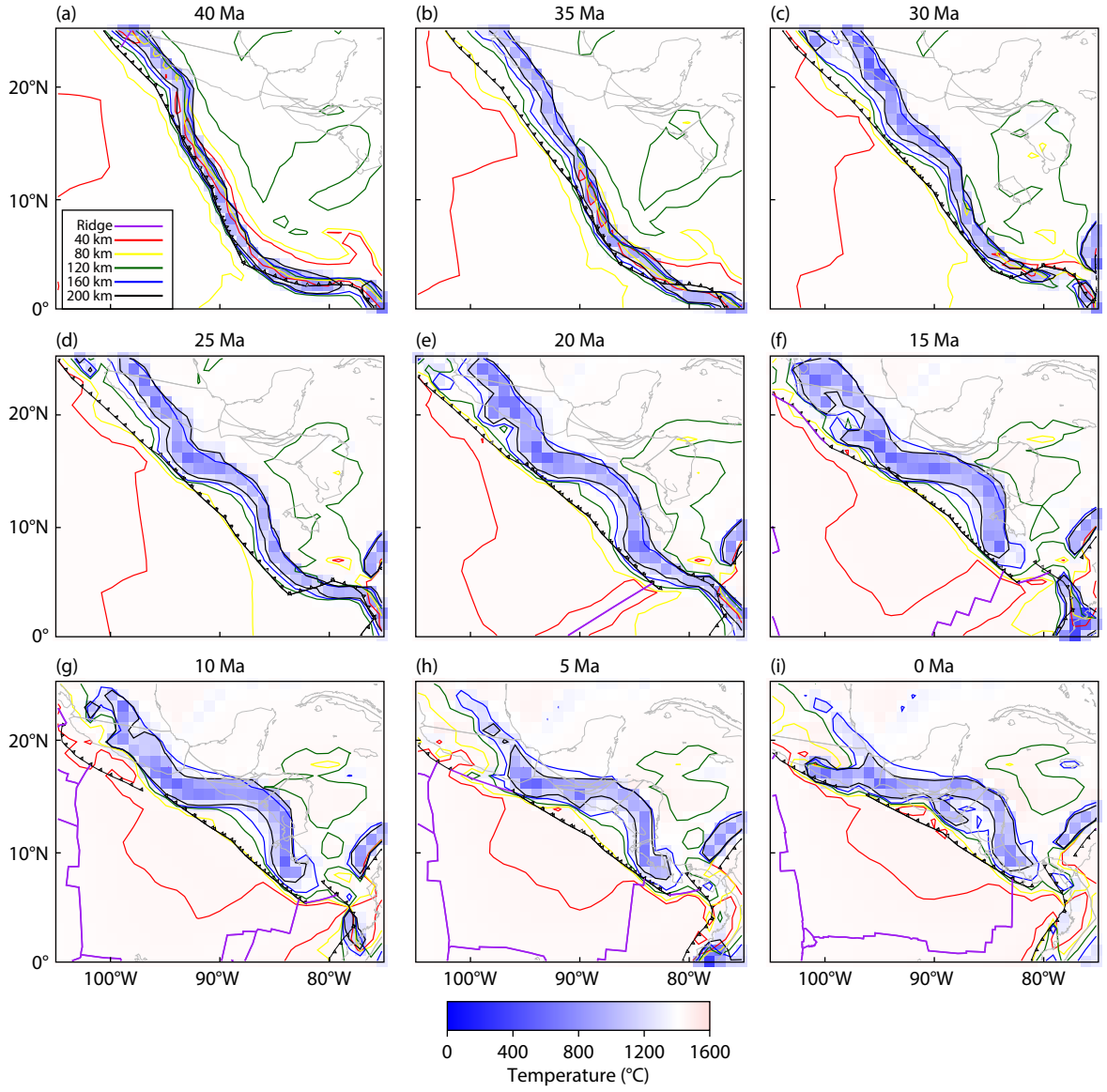

Figure 4. Evolution process of Model 2 (with the Farallon slab). The legend and color scale are the same as those in Figure 3.

segments; Figure 7). When seen through the blurry tomographic lens, the folded slab doublets could appear as an ultra-thick slab pile at upper-mantle depths (Figure 1) that is difficult to explain with the traditional single-slab model.

Although tearing of the subducting slab is strongly controlled by the flow effect of the "mantle wind," this process needs to be evaluated within the context of the regional geological background of Central America. In our model, slab tearing occurs at three key locations. The first is the gap that initially opened on the northern side. Unlike the vertical tearing mechanisms previously identified, such as a sudden change in the subduction angle of the Cocos slab (Dougherty et al., 2020; Calò, 2021) or the retreat of the subducting slab (Dougherty and Clayton, 2014; Castellanos et al., 2018), we propose that the northern tearing is controlled by the 3D mantle flow driven by both the pressure gradient that generates the poloidal flow component and the northern edge of the Cocos slab that forms the toroidal flow component, as can be seen from the progressively enlarged tear size toward the northern boundary.

The second location of slab tear is the central part of the trench west of present-day Nicaragua and Honduras, where tears emerge around 5 million years ago (5 Ma). The style of slab tearing in this region depends mostly on the lateral pressure gradient (Figure 2) because of the existence of the ancient Farallon slab. By incorporating the Farallon slab, the depth of the tear becomes shallower. In Model 1, the tear mainly forms at depths of 80–120 km, whereas in Model 2, the gap starts to appear at approximately 40 km depth. We attribute this difference to the sinking of the Farallon slab, which draws mantle material from the west and causes upward mantle flow (thus creating positive pressure) near the subducting slab side, leading to a shallower slab and shallower tear. Additionally, the inclusion of the Farallon slab in Model 2 alters the subduction geometry of the Cocos slab (Figures 6d–6e and 7). The broader slab tears in this model lead to more imbricated slab doublets at upper-mantle depths (Figure 6e) than those in Model 1 (Figure 6d), such that sinking of this large slab pile

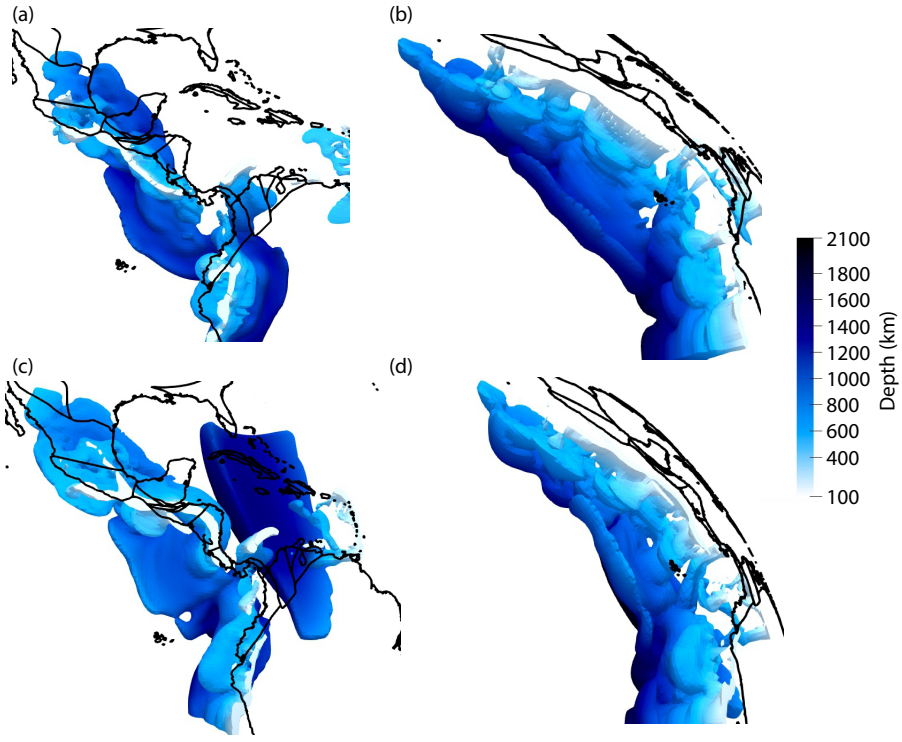

Figure 5. The 3D morphology of the present Cocos slab in the two models. Panels (a) and (b) show different views of the Cocos slab in Model 1 (excluding the ancient Farallon slab). Panels (c) and (d) present different perspectives on the Cocos slab in Model 2 (including the ancient Farallon slab). To better visualize the slab geometry, the top 200 km of the Earth's surface has been removed in all figures.

enhances the lateral pressure gradient, thus pushing the slab further inland relative to Model 1 while maintaining shallow slab tears. We conclude that this self-reinforcing mechanism is the primary driver for the slab to tear.

The third location is the slab window that opens in the southern part of the study area, where the Cocos Ridge subducts (Figures 6f–6g). Previous studies have suggested that the slab window in this region is formed by continuous spreading during ridge subduction (Johnston and Thorkelson, 1997; Abratis and Wörner, 2001; McGirr et al., 2021). We find that the opening of this slab window is also influenced by the mantle wind (Peng DD et al., 2021a; Li YC et al., 2024), when the Farallon slab draws mantle material northeastward and enlarges the slab window. This demonstrates that the lateral pressure gradient also influences dynamics near the slab edges.

It is worth noting that the magnitude of the dynamic pressure is only a few tens of megapascals (Figure 2), which is much smaller than the intraplate stress attributable to the negative buoyancy of the slab. However, the intraplate stress is highly localized within the slab. Because the Cocos slab is very young, it results in relatively small intraslab stress so that the prominent deformation occurs only within the cold core of the thin slab. In contrast, the dynamic pressure is much more widespread and consistently acting on the two surfaces of the slab. When integrating these two stress types over the volume, their magnitudes may become comparable. In addition, these two forces act differently in shaping the slab morphology. The self-gravity tends to thin and even tear the slab in the vertical direction, whereas the dynamic pressure acts more laterally and tends to shift the slab inland, thus helping to reduce the slab dip angle and enlarge the slab tear.

Our model results confirm that the self-gravitational stress of the slab does play an important role in deforming the Cocos slab, as evidenced by the smaller tear even in models without the remnant Farallon slab (Figures 3 and 5a–5b). However, when the residual Farallon slab is further included, slab tearing initiates earlier, with larger and more persistent gaps (Figures 4 and 5c–5d). Because the latter case results in a more landward position of the slab, forming two separate slab branches as seismically imaged, we conclude that this particular slab behavior is primarily driven by the lateral pressure gradient (mantle wind) generated by the sinking residual Farallon slab.

In summary, this study establishes a four-dimensional data assimilation model for the Central American subduction zone to investigate the influence of former subduction on slab evolution since the Eocene. We find that slab tears observed at different locations in the region are influenced to varying degrees by lateral mantle flow (mantle wind) induced by the sinking Farallon slab on the east. The repeated tearing and sinking of the Cocos slab explains the enigmatic mantle structures below the region (Figure 7).

Acknowledgments

This work is supported by the Strategy Priority Research Program (Category B) of the Chinese Academy of Sciences (Grant No. XDB0710000) and the National Natural Science Foundation of China (Grant No. 92355302). The computations were supported by the National Supercomputer Center in Tianjin.

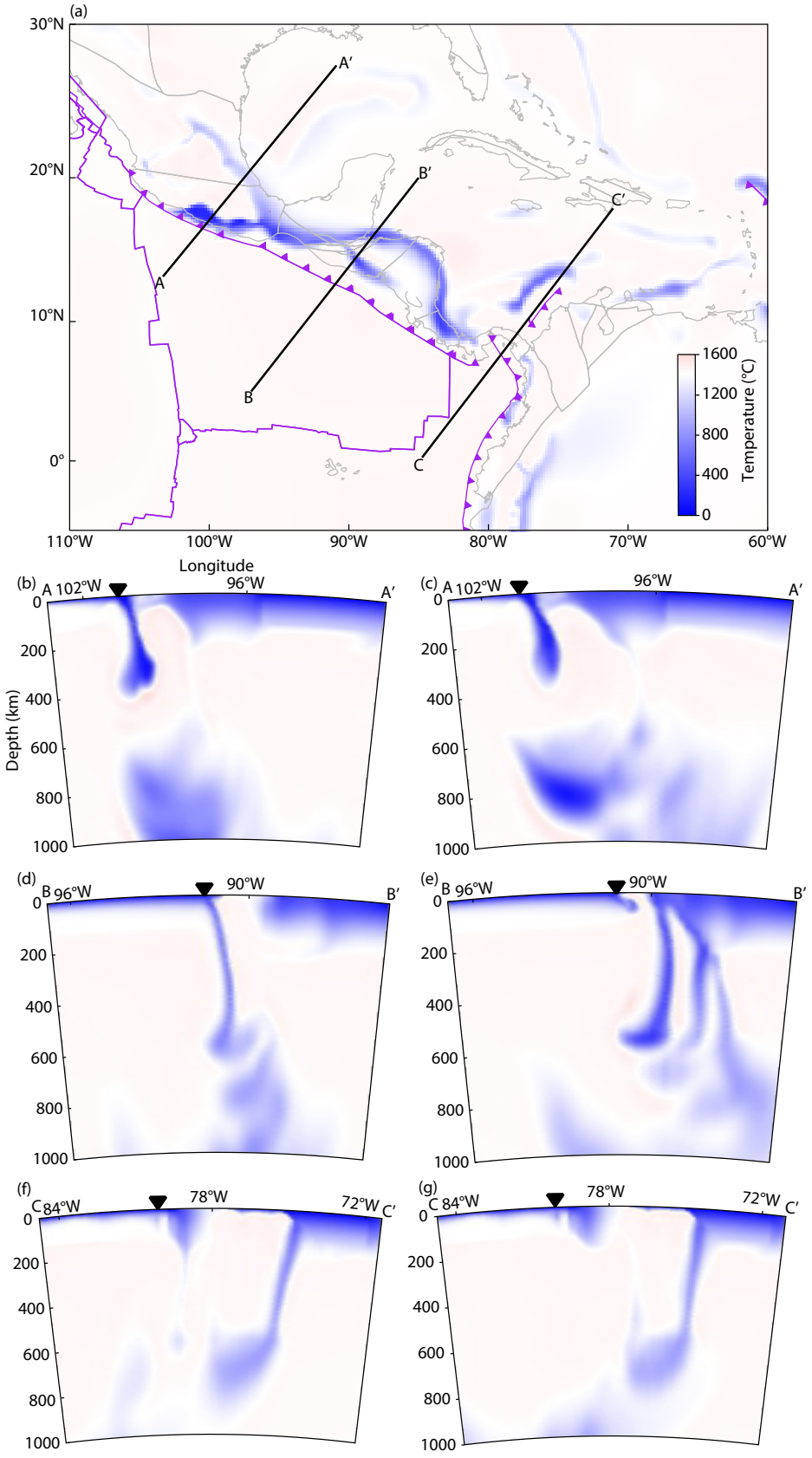

Figure 6. Cross-sectional views of the temperature field in Central America. (a) Locations of three trench-normal cross-sections, with the background displaying the temperature field at 200 km depth from Model 2. Panels (b) and (c) display the cross-sectional temperature field along A–A′ for Model 1 and Model 2, respectively. Panels (d) and (e) display the cross-sectional temperature along B–B′ for Model 1 and Model 2, respectively. Panels (f) and (g) display the cross-sectional temperature along C–C′ for Model 1 and Model 2, respectively.

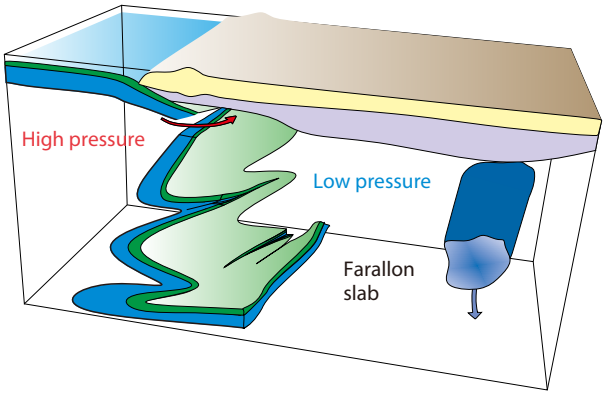

Figure 7. Schematic illustration of how the pressure gradient controls slab evolution in Central America. The lateral pressure gradient-driven mantle wind tears the subducting Cocos slab, simultaneously opening a pathway for mantle material to flow into the mantle wedge. The 3D arrows represent the direction of the mantle wind through the slab tear.

References

Abratis, M., and Wörner, G. (2001). Ridge collision, slab-window formation, and the flux of Pacific asthenosphere into the Caribbean realm. *Geology*, *29*(2), 127–130. https://doi.org/10.1130/0091-7613(2001)029<0127:RCSWFA>2.0.CO;2

Calò, M. (2021). Tears, windows, and signature of transform margins on slabs. Images of the Cocos plate fragmentation beneath the Tehuantepec isthmus (Mexico) using Enhanced Seismic Models. *Earth Planet. Sci. Lett.*, *560*, 116788. https://doi.org/10.1016/j.epsl.2021.116788

Castellanos, J. C., Clayton, R. W., and Pérez-Campos, X. (2018). Imaging the eastern trans-Mexican volcanic belt with ambient seismic noise: Evidence for a slab tear. *J. Geophys. Res.: Solid Earth*, *123*(9), 7741–7759. https://doi.org/10.1029/2018JB015783

Dougherty, S. L., and Clayton, R. W. (2014). Seismicity and structure in central Mexico: Evidence for a possible slab tear in the South Cocos plate. *J. Geophys. Res.: Solid Earth*, *119*(4), 3424–3447. https://doi.org/10.1002/2013JB010883

Dougherty, S. L., Jiang, C. X., Clayton, R. W., Schmandt, B., and Hansen, S. M. (2020). Seismic evidence for a fossil slab origin for the Isabella anomaly. *Geophys. J. Int.*, *224*(2), 1188–1196. https://doi.org/10.1093/gji/ggaa472

Gianni, G. M., Navarrete, C., and Spagnotto, S. (2019). Surface and mantle records reveal an ancient slab tear beneath Gondwana. *Sci. Rep.*, *9*(1), 19774. https://doi.org/10.1038/s41598-019-56335-9

Grand, S. P., van der Hilst, R. D., and Widiyantoro, S. (1997). Global seismic tomography: A snapshot of convection in the Earth. *GSA Today*, *7*(4), 1–7.

Hawley, W. B., and Allen, R. M. (2019). The fragmented death of the Farallon plate. *Geophys. Res. Lett.*, *46*(13), 7386–7394. https://doi.org/10.1029/2019GL083437

Hayes, G. P., Moore, G. L., Portner, D. E., Hearne, M., Flamme, H., Furtney, M., and Smoczyk, G. M. (2018). Slab2, a comprehensive subduction zone geometry model. *Science*, *362*(6410), 58–61. https://doi.org/10.1126/science.aat4723

Hu, J. S., Liu, L. J., Hermosillo, A., and Zhou, Q. (2016). Simulation of Late Cenozoic South American flat-slab subduction using geodynamic models with data assimilation. *Earth Planet. Sci. Lett.*, *438*, 1–13. https://doi.org/10.1016/j.epsl.2016.01.011

Hu, J. S., Faccenda, M., and Liu, L. J. (2017). Subduction-controlled mantle flow and seismic anisotropy in South America. *Earth Planet. Sci. Lett.*, *470*, 13–24. https://doi.org/10.1016/j.epsl.2017.04.027

Hu, J. S., Liu, L. J., and Zhou, Q. (2018). Reproducing past subduction and mantle flow using high-resolution global convection models. *Earth Planet. Phys.*, *2*(3), 189–207. https://doi.org/10.26464/epp2018019

Hyndman, R. D., Yamano, M., and Oleskevich, D. A. (1997). The seismogenic zone of subduction thrust faults. *Isl. Arc*, *6*(3), 244–260. https://doi.org/10.1111/j.1440-1738.1997.tb00175.x

Johnston, S. T., and Thorkelson, D. J. (1997). Cocos-Nazca slab window beneath Central America. *Earth Planet. Sci. Lett.*, *146*(3-4), 465–474. https://doi.org/10.1016/S0012-821X(96)00242-7

Jolivet, L., Menant, A., Sternai, P., Rabillard, A., Arbaret, L., Augier, R., Laurent, V., Beaudoin, A., Grasemann, B., … Le Pourhiet, L. (2015). The geological signature of a slab tear below the Aegean. *Tectonophysics*, *659*, 166–182. https://doi.org/10.1016/j.tecto.2015.08.004

Kim, Y., Clayton, R. W., and Keppie, F. (2011). Evidence of a collision between the Yucatán Block and Mexico in the Miocene. *Geophys. J. Int.*, *187*(2), 989–1000. https://doi.org/10.1111/j.1365-246X.2011.05191.x

Li, Y. C., Liu, L. J., Li, S. Z., Peng, D. D., Cao, Z. B., and Li, X. Y. (2024). Cenozoic India-Asia collision driven by mantle dragging the cratonic root. *Nat. Commun.*, *15*(1), 6674. https://doi.org/10.1038/s41467-024-51107-0

Liu, L. J., Spasojević, S., and Gurnis, M. (2008). Reconstructing Farallon plate subduction beneath North America back to the Late Cretaceous. *Science*, *322*(5903), 934–938. https://doi.org/10.1126/science.1162921

Liu, L. J., and Stegman, D. R. (2011). Segmentation of the Farallon slab. *Earth Planet. Sci. Lett.*, *311*(1-2), 1–10. https://doi.org/10.1016/j.epsl.2011.09.027

Liu, L. J., and Stegman, D. R. (2012). Origin of Columbia River flood basalt controlled by propagating rupture of the Farallon slab. *Nature*, *482*(7385), 386–389. https://doi.org/10.1038/nature10749

Liu, M., and Gao, H. Y. (2023). Role of subduction dynamics on the unevenly distributed volcanism at the Middle American subduction system. *Sci. Rep.*, *13*(1), 14697. https://doi.org/10.1038/s41598-023-41740-y

McGirr, R., Seton, M., and Williams, S. (2021). Kinematic and geodynamic evolution of the Isthmus of Panama region: Implications for Central American seaway closure. *GSA Bull.*, *133*(3-4), 867–884. https://doi.org/10.1130/B35595.1

Miller, M. S., Gorbatov, A., and Kennett, B. L. N. (2006). Three-dimensional visualization of a near-vertical slab tear beneath the southern Mariana arc. *Geochem. Geophys. Geosyst.*, *7*(6), Q06012. https://doi.org/10.1029/2005GC001110

Müller, R. D., Zahirovic, S., Williams, S. E., Cannon, J., Seton, M., Bower, D. J., Tetley, M. G., Heine, C., Le Breton, E., … Gurnis, M. (2019). A global plate model including lithospheric deformation along major rifts and Orogens since the Triassic. *Tectonics*, *38*(6), 1884–1907. https://doi.org/10.1029/2018TC005462

Obayashi, M., Yoshimitsu, J., and Fukao, Y. (2009). Tearing of stagnant slab. *Science*, *324*(5931), 1173–1175. https://doi.org/10.1126/science.1172496

Obrebski, M., Allen, R. M., Xue, M., and Hung, S. H. (2010). Slab-plume interaction beneath the Pacific Northwest. *Geophys. Res. Lett.*, *37*(14), L14305. https://doi.org/10.1029/2010GL043489

Peng, D. D., Liu, L. J., Hu, J. S., Li, S. Z., and Liu, Y. M. (2021a). Formation of East Asian stagnant slabs due to a pressure-driven Cenozoic mantle wind following Mesozoic subduction. *Geophys. Res. Lett.*, *48*(18), e2021GL094638. https://doi.org/10.1029/2021GL094638

Peng, D. D., Liu, L. J., and Wang, Y. Y. (2021b). A newly discovered Late-Cretaceous East Asian flat slab explains its unique lithospheric structure and tectonics. *J. Geophys. Res.: Solid Earth*, *126*(10), e2021JB022103. https://doi.org/10.1029/2021JB022103

Peng, D. D., and Liu, L. J. (2022). Quantifying slab sinking rates using global geodynamic models with data-assimilation. *Earth-Sci. Rev.*, *230*, 104039. https://doi.org/10.1016/j.earscirev.2022.104039

Rogers, R. D., Kárason, H., and van der Hilst, R. D. (2002). Epeirogenic uplift above a detached slab in northern Central America. *Geology*, *30*(11), 1031–1034. https://doi.org/10.1130/0091-7613(2002)030<1031:EUAADS>2.0.CO;2

Schmandt, B., and Humphreys, E. (2010). Complex subduction and small-scale convection revealed by body-wave tomography of the western United States upper mantle. *Earth Planet. Sci. Lett.*, *297*(3-4), 435–445. https://doi.org/10.1016/j.epsl.2010.06.047

Stolper, E., and Newman, S. (1994). The role of water in the petrogenesis of Mariana trough magmas. *Earth Planet. Sci. Lett.*, *121*(3-4), 293–325. https://

doi.org/10.1016/0012-821X(94)90074-4

Tackley, P. J., and King, S. D. (2003). Testing the tracer ratio method for modeling active compositional fields in mantle convection simulations. *Geochem. Geophys. Geosyst.*, *4*(4), 8302. https://doi.org/10.1029/2001GC000214

Tan, E., Choi, E., Thoutireddy, P., Gurnis, M., and Aivazis, M. (2006). GeoFramework: Coupling multiple models of mantle convection within a computational framework. *Geochem. Geophys. Geosyst.*, *7*(6), Q06001. https://doi.org/10.1029/2005GC001155

Xue, T., Peng, D. D., Liu, K. H., Obrist-Farner, J., Locmelis, M., Gao, S. S., and Liu, L. J. (2023). Ongoing fragmentation of the subducting Cocos slab, Central America. *Geology*, *51*(12), 1106–1110. https://doi.org/10.1130/G51403.1

Zhong, S. J., Zuber, M. T., Moresi, L., and Gurnis, M. (2000). Role of temperature-dependent viscosity and surface plates in spherical shell models of mantle convection. *J. Geophys. Res.: Solid Earth*, *105*(B5), 11063–11082. https://doi.org/10.1029/2000JB900003

Zhou, Q., Hu, J. S., Liu, L. J., Chaparro, T., Stegman, D. R., and Faccenda, M. (2018a). Western, U.S. seismic anisotropy revealing complex mantle dynamics. *Earth Planet. Sci. Lett.*, *500*, 156–167. https://doi.org/10.1016/j.epsl.2018.08.015

Zhou, Q., Liu, L. J., and Hu, J. S. (2018b). Western US volcanism due to intruding oceanic mantle driven by ancient Farallon slabs. *Nat. Geosci.*, *11*(1), 70–76. https://doi.org/10.1038/s41561-017-0035-y

Zhu, H. J., Stern, R. J., and Yang, J. D. (2020). Seismic evidence for subduction-induced mantle flows underneath Middle America. *Nat. Commun.*, *11*(1), 2075. https://doi.org/10.1038/s41467-020-15492-6